PCCP

Accepted Manuscript

ROYAL SOCIETY OF CHEMISTRY

www.rsc.org/pccp

Structural origin of the unusual compression behaviors in nanostructured TiO_2: Insights from first-principles calculations

Varghese Swamy[a,b*]

ABSTRACT

First-principles calculations of anatase structured TiO_2 and ZrO_2 as well as of TiO_2-B were carried out to 20 GPa in order to develop an understanding of the unusual compression and pressure-dependent phase transitions reported for nanocrystalline (nc) pure and Zr-doped anatase and nc TiO_2-B. The computations, carried out using two global hybrid density functional–Hartree-Fock formulations and all-electron basis sets, reveal sharp lattice hardening along the crystallographic *a* direction and concurrent lattice softening along *c* for anatase TiO_2 at 10-12 GPa, and smooth anisotropic compression for ZrO_2 anatase. Significant structural changes beginning ~10 GPa are also predicted for TiO_2-B, most dramatically shown by the pressure-dependent change in the monoclinic angle β. These structural changes, resulting from *intrinsic* crystal structure destabilizations under extended pressure metastability, have been suggested as responsible for the unusual mechanical behaviors reported for pure and Zr-doped nanocrystalline and microcrystalline anatase TiO_2 and nc TiO_2-B.

Keywords: TiO_2 and ZrO_2 anatase, TiO_2-B, global hybrid density functionals, high pressure, equation of state, amorphization

1. Introduction

Anatase TiO_2 is currently one of the most widely investigated oxides principally because of the exceptional photocatalytic and photovoltaic properties that can be realized by tailoring its size, morphology, and chemistry.[1-3] Significant advances are being made in the understanding of the atomic configurations and physical-chemical interactions at reduced and finite dimensions of the anatase crystal structure by employing first-principles calculations and sophisticated experiments.[4-9] Nanostructured rutile is relatively less investigated while nc TiO_2-B is gaining attention as a negative electrode material for rechargeable lithium-ion batteries.[10,11] The burgeoning interest in nc TiO_2 has uncovered a host of unique and intriguing size-dependent behaviors, including unusual compression and pressure-driven phase transitions. Room-temperature compression studies of nc anatase have suggested strong size-, morphology-, and growth direction-dependencies of its phase transitions and compressibility.[12-18] Crystallite size-dependent pressure-induced post-anatase transformations to amorphous TiO_2 (< 10 nm), monoclinic baddeleyite TiO_2 (~10-50 nm), and orthorhombic α-PbO_2 structured TiO_2 (>50 nm) were suggested.[19] Furthermore, a pressure-driven high-density amorphous (HDA) – low density amorphous (LDA) *polyamorphic* transition was demonstrated for the pressure-amorphized nc anatase.[20] Size-related enhanced structure metastability under pressure and compressibility variations in nc anatase have also been widely investigated,[12-20] leading to the recognition of a non-monotonous compression curve for a 6-nm-anatase showing abrupt stiffness enhancement around 10-12 GPa.[21]

In addition to size-control, attempted composition-tuning of the mechanical properties of nc anatase via Zr-doping produced apparently counterintuitive results. The pressure (P)–volume (V) equation of state (EoS) for a 15±5 nm $Ti_{0.9}Zr_{0.1}O_2$ anatase yielded zero-pressure bulk

modulus (K_o) values of 213±9, 221, 266±6 GPa, etc with pressure derivative (K') values in the range of 15.5–17.9, depending on the P-range considered or fitting method used.[22] The large K_o = 266±6 GPa is contrary to that expected in a Zr-doped anatase (of the known isostructural TiO_2 and ZrO_2 phases, the former are relatively stiffer), and the extremely large pressure derivative values are highly unusual ($K' \approx 4$ for most materials). Large stiffness increase following multiple compressions was also reported for a 12±3 nm $Ti_{0.9}Zr_{0.1}O_2$ anatase.[23]

Nanoribbon-structured single crystalline TiO_2-B was also reported to undergo pressure-induced amorphization (PIA) to an HDA TiO_2 around 16 GPa and further HDA→LDA polyamorphic transition upon decompression from high-pressures to about 8.1 GPa,[24] in a very similar fashion to nc anatase.[20] It is noteworthy that PIA has not been observed in nc rutile[15] and not reported for nc brookite. An explanation for the contrasting pressure-dependent behaviors of anatase and TiO_2-B on the one hand, and rutile and brookite on the other, remains elusive. The first-principles calculations of bulk anatase-structured TiO_2 and ZrO_2 as well as of TiO_2-B presented in this work suggest that the unusual compression and phase transition behaviors of pure and Zr-doped nc anatase as well as of nc TiO_2-B result largely from inherent structure destabilizations under metastable high pressure regimes.

2. Computational Methods

The calculations were performed within the B3LYP[25-26] and PBE0[27] global hybrid Hartree-Fock–density functional theory (HF-DFT) formulations using the CRYSTAL09[28-29] package. The details of the computations employing all–electron linear combination of atom-centered orbitals (AE-LCAO) approach are same as in reference 30.The following Gaussian-type orbitals (GTO) basis sets were used for Ti and O: the triple valence all-electron (TVAE) basis sets[31]; the pob-TZVP basis sets,[32] and the Ti_86-411(d31)[33] and O_8-411d1_bredow_2006

basis set.[34] The results obtained with the latter two basis sets are similar to that calculated using TVAE. Therefore, only the TVAE results are presented for TiO_2. For ZrO_2 the Dovesi *et al*.[35] all-electron GTO Zr basis set and the pob-TZVP O basis set were used.

The reciprocal space integration was carried out by sampling the Brillouin zone using Monkhorst-Pack grids with a shrinking factor of 8. The accuracy of the computational results in CRYSTAL09 is determined by five truncation criteria for bielectronic integrals (Coulomb and exchange series) labeled ITOL1, ITOL2, ITOL3, ITOL4, and ITOL5 (see ref. 29). The present study used values of 10^{-9}, 10^{-9}, 10^{-9}, 10^{-9}, and 10^{-18}, respectively for the above truncation criteria (these values are much higher than the default values). Structure optimizations used the following very strict convergence criteria with energy thresholds (in a.u.) for SCF convergence of 10^{-9} and 10^{-10}, and for geometry optimization 10^{-9} in all the calculations.

For a given external pressure, the enthalpy function $H = E + PV$ was minimized using analytical gradients with respect to the internal and external coordinates. Here H is the enthalpy, E internal energy, and V the unit cell volume.

The following third-order Birch-Murnaghan equation of state[36,37] was used to extract the isothermal equation of state parameters from the P-V data:

$$P = 1.5K_o [(V_o/V)^{7/3} - (V_o/V)^{5/3}] \times \{1 - 0.75 (4 - K') \times [(V_o/V)^{2/3} - 1]\} \quad (1)$$

3. Results and Discussion

The optimized 0 GPa structures of anatase TiO_2, fictive anatase ZrO_2, and TiO_2-B are presented in Fig. 1 and Tables 1-2. The computed structures are in very good agreement with published experimental data for anatase TiO_2[42] and TiO_2-B.[39] Similarly, the computed fictive ZrO_2 anatase structure is very close to the planewave-pseudopotential (PW-Psp) local density approximation result[43] (see Table 1). The extreme sensitivity of the anatase TiO_2 structure, especially the lattice constant *c*, to the choice of exchange-correlation functionals such as HF, local density, and generalized gradient approximations (GGA) is well documented.[31,38] In order to illustrate the quality of the present results, a comparison of the experimental data with the present B3LYP calculations shows deviations of 0.6%, 1.6%, and 2.63% for *a*, *c*, and *V* from experimental data,[42] in better agreement than recent GGA[40] and hybrid functionals[38,44] predictions.

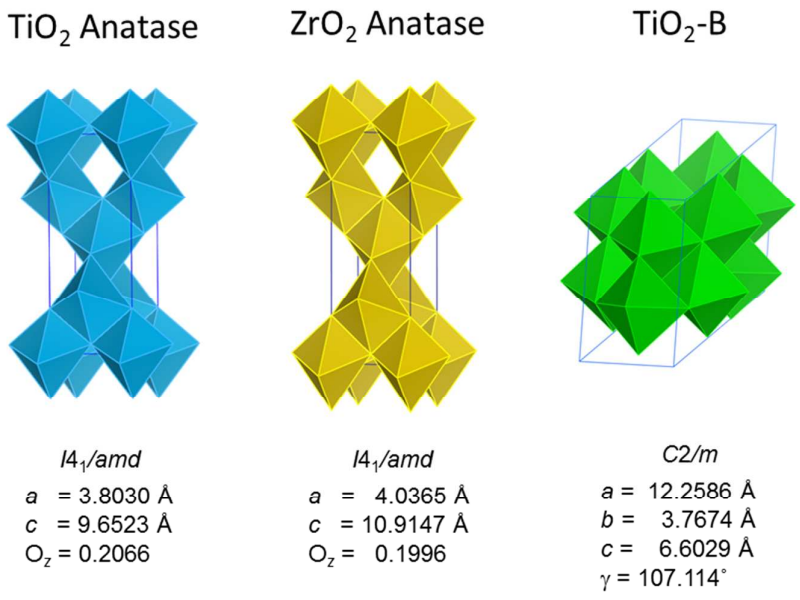

Fig. 1 Polyhedral representation of the computed (B3LYP hybrid functional, TVAE basis sets) crystal structures at 0GPa.The atomic coordinates computed for TiO_2-B are given in Table 2.

The unit cell volume for anatase TiO_2 and ZrO_2 calculated using B3LYP are shown in Fig. 2. Experimental unit cell volume for 15 nm anatase TiO_2 and 12 nm anatase $Ti_{0.9}Zr_{0.1}O_2$ are also plotted. The present results suggest that complete substitution of larger Zr^{4+} (0.72 nm) for Ti^{4+} (0.61 nm) in the anatase structure expands the unit cell (Fig. 1) and diminishes the K_o value (see Table 3 below), consistent with data for other TiO_2 and ZrO_2 phases. For nc TiO_2-$Ti_{0.9}Zr_{0.1}O_2$ anatase, a parallel behaviour is seen in the Vegard's law trend for experimental V_o (Fig. 2), but not in the experimental K_o data (see Table 3 below), suggesting the effects of nanocrystallinity as discussed later.

Table 1. Computed and Experimental Crystal Structures of Anatase TiO_2 and ZrO_2

Phase	Method	*a* (Å)	*c* (Å)	*u*	V_o (Å^3)	Reference
TiO_2	AE-LCAO-B3LYP-TVAE	3.803	9.652	0.207	139.599	this study
	AE-LCAO-PBE0-TVAE	3.777	9.559	0.207	136.323	this study
	PBE0	3.758	9.704	0.204	137.045	ref 38
	AE-LCAO-B3LYP	3.791	9.758	0.205	140.239	ref 39
	PAW-PBE	3.803	9.769	0.206	141.287	ref 39
	AE-LCAO-B3LYP	3.783	9.805	0.204	140.320	ref 38
	FP-LAPW-GGA	3.838	9.643	0.209	142.036	ref 40
	PW-PAW-10	3.804	9.724	0.206	140.710	ref 41
	PW-PAW-4	3.810	9.726	0.206	141.184	ref 41
	AE-LCAO-GGA	3.794	9.712	0.206	139.799	ref 31
	PW-Psp-GGA	3.792	9.714	0.206	139.680	ref 31
	Experiment (at 15 K)	3.782	9.502	0.208	135.927	ref 42
ZrO_2	AE-LCAO-B3LYP	4.036	10.915	0.200	177.832	this study
	AE-LCAO-PBE0	4.004	10.853	0.199	174.023	this study
	PW-Psp-LDA	4.095	10.659	0.203	178.741	ref 43

Table 2. Computed and Experimental Crystal Structure of TiO_2-B

Parameter	B3LYP	PBE0	Experiment[39]
a **(Å)**	12.2586	12.1905	12.197(8)
b **(Å)**	3.7674	3.7471	3.7537(15)
c **(Å**	6.6029	6.5208	6.535(4)
β **(°)**	107.114	107.134	107.16(8)
V_o **(Å^3)**	291.44	284.64	285.9(2)
Ti1$_{(x)}$	0.1943	0.1953	0.193(3)
Ti1$_{(z)}$	0.2812	0.2838	0.287(4)
Ti2$_{(x)}$	0.1006	0.1007	0.100(2)
Ti2$_{(z)}$	-0.2908	-0.2922	-0.291(4)
O1$_{(x)}$	0.1326	0.1339	0.131
O1$_{(z)}$	0.0028	0.0036	0.004
O2$_{(x)}$	-0.2360	-0.2367	-0.238
O2$_{(z)}$**)**	-0.3405	-0.3442	-0.346
O3$_{(x)}$	0.0590	0.0587	0.059
O3$_{(z)}$	0.3715	0.3713	0.373
O4$_{(x)}$	-0.1386	-0.1384	-0.140
O4$_{(z)}$	0.2952	0.2966	0.290

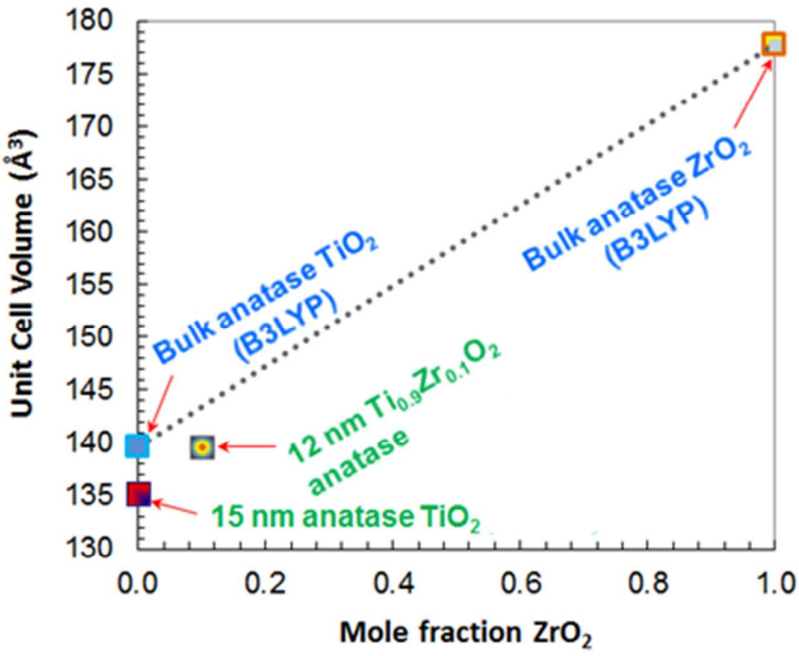

Fig. 2 Calculated (B3LYP) unit cell volume for bulk anatase TiO_2 and ZrO_2. Experimental unit cell volume data for 15 nm anatase TiO_2 (ref 16) and 12 nm anatase $Ti_{0.9}Zr_{0.1}O_2$ (ref 23) are also plotted.

The calculated pressure-dependencies of the unit cell parameters and metal-oxygen bond lengths for the three structures are presented in Fig. 3 along with available experimental data for anatase TiO_2. The EoS parameters derived by fitting the *P*–*V* data of this study are compared with available experimental and theoretically obtained data from the literature in Table 3. For anatase TiO_2, the present results are in excellent agreement with that determined using *in situ* XRD, especially that for polycrystalline anatase.[45] For ZrO_2 anatase, while V_o is very similar, the K_o and K' values of this study are slightly smaller in relation to previous prediction with planewave pseudopotential local density approximation.[43]

The most striking feature of the predicted pressure evolutions of the lattice parameters, not reported in any previous first-principles study,[22,31,44,45,48,49] is the distinct change in compression at ~12 GPa for TiO_2 anatase: at this pressure, the lattice stiffens abruptly at an

increased rate along *a* while concurrently becomes more compliant along *c* (Fig. 3a). In contrast to anatase TiO_2, the calculated anatase ZrO_2 (Fig. 3b) displays what may be considered a normal lattice compression behavior. The pressure-dependencies of the computed TiO_2-B structure parameters (Fig. 3c) also show unusual trends, especially β with a sharp increase beginning around 10 GPa.

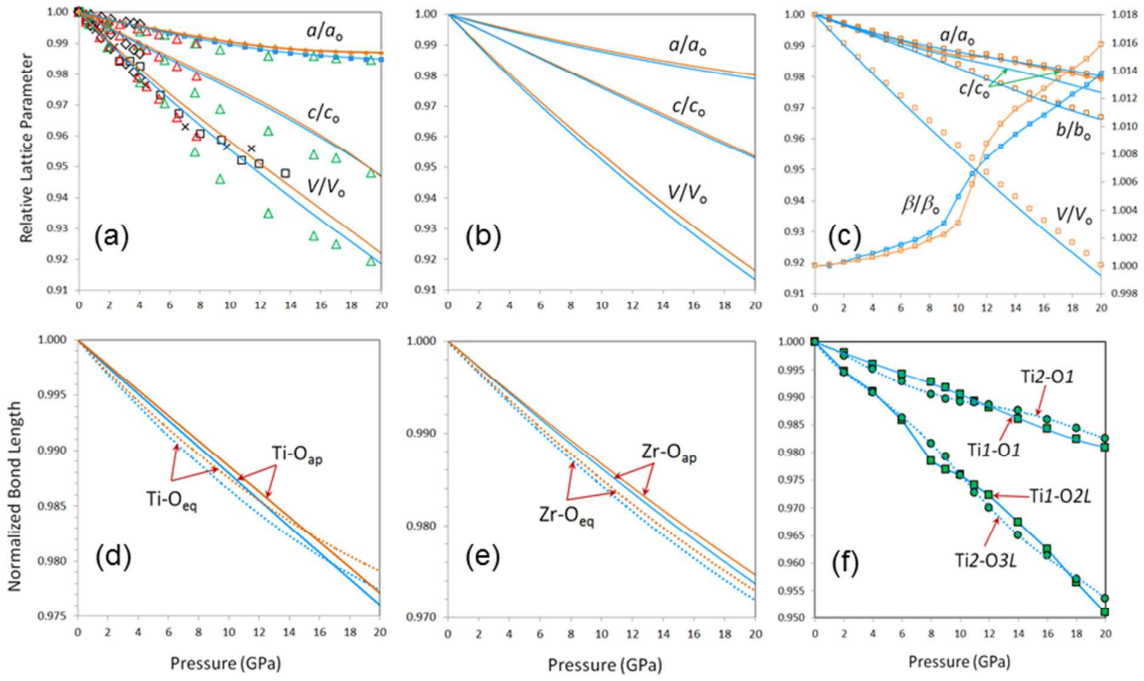

Fig. 3 Calculated (B3LYP-blue, PBE0-orange) pressure dependent crystal structure changes in anatase TiO_2 (a, d), anatase ZrO_2 (b, e), and TiO_2-B (c, f). (a) green triangle - 6 nm anatase (ref 21); red triangle – microparticle anatase (ref 46); cross and square – microparticle anatase (ref 45); diamond – single crystal anatase (ref 45). Metal-oxygen bond lengths were computed using VESTA.[47]

Table 3. Zero-Pressure EoS Parameters for (Ti,Zr)O_2 Anatase and TiO_2-B

Phase	Method	V_o (Å^3)	K_o (GPa)	K'	Reference
TiO_2	AE-LCAO-B3LYP	139.601±003	197.26±0.45	4.74±0.92	this study
	AE-LCAO-PBE0	136.331±0.09	210.35±1.49	5.07±0.31	this study
	FP-LAPW-GGA	142.0362[a]	199.6355	4.0[b]	ref 40
	AE-LCAO-B3LYP	141.36	200.34	2.538	ref 44
	PW-PAW-GGA	NA[c]	189, 199	NA	ref 41
	XRD (single crystal)	136.277±5	179±2	4.5±10	ref 45
	XRD (microcrystal)	NA	190±10	5.3±10	ref 45
	XRD (microcrystal)	136.74±5	178±1	4.0	ref 46
	XRD (nanocrystal)	variable[d]	243±3, 237±7, 204±8–319±20[d], 185±2.6[d]–245±4.2	variable	refs 12-14,16
ZrO_2	AE-LCAO-B3LYP	177.823±0.011	188.28±1.07	3.54±0.21	this study
	AE-LCAO-PBE0	174.031±0.008	197.75±1.21	3.25±0.24	this study
	PW-LDA-Psp	178.74	209	4.63	ref 43
$Ti_{0.9}Zr_{0.1}O_2$	XRD (15±5, 12±3 nm)	139.6, 139.3±1	211±7[e]–278±7	15.5 – 17.9±2	refs 22,23
	XRD (15±5 nm)	139.53±0.04	251.58±4.32	4.0[f]	this study[g]
	XRD (12±3 nm)	139.40±0.14	210.58±11.09	4.0[f]	this study[h]
	XRD (12±3 nm)	138.40±0.06	198.76±3.04	4.0[f]	this study[i]
TiO_2-B	AE-LCAO-B3LYP	291.48±0.03	198.91±0.83	4.0[f]	this study
	AE-LCAO-PBE0	284.64±0.012	214.18±0.36	4.0[f]	this study

[a]Calculated from unit cell parameters; [b]K' not explicitly mentioned; [c]NA – not available in the source; [d]strongly size- or shape-dependent; [e]only compression data considered (see text); [f]second-order Birch-Murnaghan EoS fit to data at P <8 GPa (see text); [g]compression data of pre-compressed sample from ref 22; [h]compression data from ref 23; [i]decompression data from ref 23.

In fact, the lattice parameter variations with pressure reflect the metal-oxygen bond length changes within the coordination polyhedra (four-edge-shared TiO_6 or ZrO_6 octahedra with elongation parallel to *c* in anatase and complex distorted Ti-O polyhedra in TiO_2-B) of the structures. Thus, the opposite "bowing" trends shown by the Ti-O bond lengths in the anatase TiO_2 structure (Fig. 3d) are due to the decrease in compressibility of the shorter (*e.g.*, 1.95 Å at 0 GPa) "equatorial" Ti-O bond lengths along *a* and concurrent increase in compressibility for the longer (1.99 Å at 0 GPa) "apical" Ti-O bond lengths along *c*. By contrast, the equatorial and apical Zr-O bond lengths in anatase ZrO_2 (respectively 2.09 Å and 2.18 Å at 0 GPa) display similar compressibilities with pressure (Fig. 3e).

The aforementioned bond length data suggest that the Ti-O bonds are shorter compared to the Zr-O bonds in the anatase structure. This means a greater density of atoms along the *a* axis in anatase TiO_2, as noted also in a previous study.[44] Moreover, it was suggested that the Zr-O bonds in anatase are more ionic than the Ti-O bonds.[50] Further work is necessary to establish the significance of the varied metal-oxygen bond lengths and nature of bonding to the disparate compression behaviours predicted for anatase-structured TiO_2 and ZrO_2.

The pressure-dependencies of the Ti-O bond lengths in TiO_2-B are more complex with "double bowing" trends (Fig. 3f). However, in this case also the shorter Ti1-O1 and Ti2-O1 bond lengths (*e.g.*, 1.77 Å and 1.86 Å at 0 GPa) are less compressible relative to the longer Ti1-O2*L* and Ti2-O3*L* bond lengths (0 GPa values of 2.39 Å and 2.14 Å, respectively).

The pressure range wherein unusual lattice stiffening was experimentally observed previously for a 6 nm anatase TiO_2 coincided with the pressure where *d*(004) crosses *d*(112), *d*(015) crosses *d*(211), and an abrupt change in the pressure dependence of *d*(011) occurs.[21] The pressure-dependency trends of lattice spacings computed for bulk anatase TiO_2 in this study

also show similar behavior, albeit at slightly higher pressures and with a slightly less conspicuous change in the pressure dependency of *d*(011) (Fig. 4).

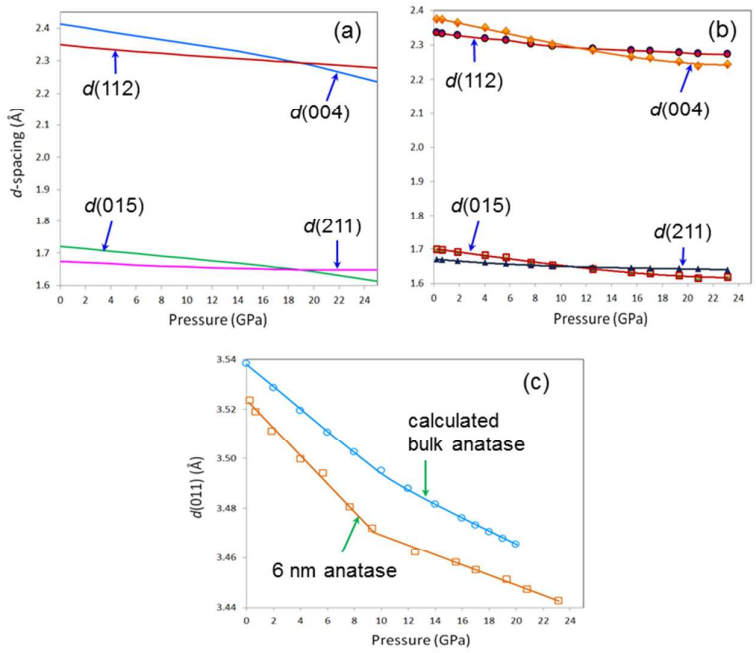

Fig. 4 Calculated (a) pressure-dependent variations of *d*(112), *d*(004), *d*(015), and *d*(211) in bulk anatase TiO_2 and corresponding experimental data (ref 21) for 6 nm anatase TiO_2 (b). (c) Comparison of the calculated (blue) and experimental data for *d*(011).

Much of the elastic deformation occurring in the anatase TiO_2 lattice has been suggested to primarily reflect the changes to the oxygen sublattice achieved by the relatively larger displacements of oxygen atoms compared to Ti atoms under compression.[21] The concerted reduction in the (004) and (112) lattice spacings with pressure was suggested to indicate larger pressure-dependent changes in the Ti-O apical bond lengths relative to the Ti-O equatorial bond lengths. This eventually leads to the destabilization of the TiO_6 octahedra, and depending on the crystallite size, triggers either structural disorder (amorphization) or crystalline phase transitions.[20,21] It may be mentioned that the anatase crystal structure is more closely related to the TiO_2-B structure than either to rutile or brookite structure. Both the anatase and TiO_2-B structures derive from cubic close packing of oxygen atoms whereas the rutile and brookite

structures derive from a hexagonal close packed arrangement of oxygen atoms.[51] Thus, it is expected that the overall response of both anatase TiO_2 and TiO_2-B to compression will be similar. This is borne out by the very similar computed EoS parameters (Table 3) and identical pressure-induced amorphization and *polyamorphic* transitions at finite crystallite sizes for both structures (unlike those for rutile and brookite structures).

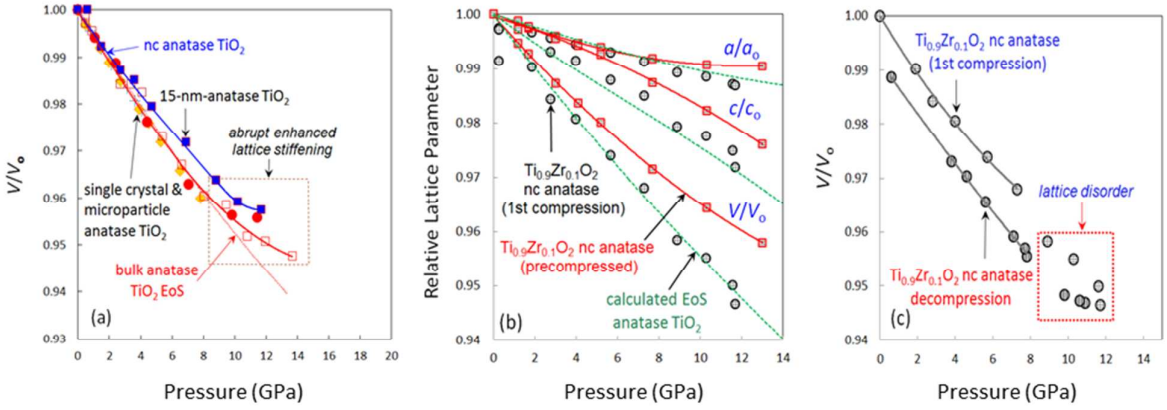

Fig. 5 Pressure dependencies of relative lattice parameters for single crystal,[45] microcrystalline,[45,46] and nc[16] anatase TiO_2 (a) and nc anatase $Ti_{0.9}Zr_{0.1}O_2$(b,c).[22,23] In (b) red square and curves represent pre-compressed 15 nm sample,[22] black circles represent 12 nm sample, and green curves represent B3LYP results. In (c) the *P-V* data of first compression and decompression of originally uncompressed material[23] are shown. Enhanced lattice hardening (a) and lattice disorder (c) are shown within the boxed area.

The experimentally observed sharp increase in lattice stiffening at ~10-12 GPa for the 6-nm anatase TiO_2 (see Fig. 4) was correlated with the onset of ~2-3 Å scale structural disorder in response to destabilization under compression of the TiO_6 octahedral arrangement.[21] In light of the present first principles calculations, we can attribute this structural destabilization to pressure-induced octahedral Ti-O bonding changes, a size-independent *intrinsic* property of the anatase TiO_2 crystal structure. This rules out previous explanations[17,22,45] of the lattice hardening as due to a sudden increase in the non-hydrostaticity of the pressure-transmitting medium (why observed only in the case of anatase TiO_2?).

For finite-sized anatase, the *P*-*V* relationship of elastic compression preceding the ~2-3 Å scale disorder[21] defines the EoS (Table 3); the mechanical behaviours of disordered anatase are distinctly different (Fig. 5). It is now possible to identify the compression-decompression data in Fig. 5c at P >8 GPa as belonging to a disordered nc anatase $Ti_{0.9}Zr_{0.1}O_2$.[21,23] The hysteretic compression–decompression paths (Fig. 5c) and smaller V_o of the decompressed 12±3 nm $Ti_{0.9}Zr_{0.1}O_2$ anatase (Table 3) suggest partial structural disorder and densification acquired within the non-elastic regime. It is suggested that the inclusion of *P*-*V* data belonging to both ordered and disordered $Ti_{0.9}Zr_{0.1}O_2$ anatase in the Birch-Murnaghan equation fit potentially led to the anomalous EoS parameters in the earlier work.[22,23] The larger K_o value obtained for the pre-compressed 15-nm $Ti_{0.9}Zr_{0.1}O_2$ anatase (Table 3) indicates contributions from both nanocrystallinity and "frozen-in" (not fully reversible) disorder.

The particle-size dependent relative contributions of bulk energy *versus* surface energy to stabilizing various crystalline and amorphous forms of TiO_2 and ZrO_2 under ambient pressure have been documented.[52,53] The relative contributions of bulk and surface energy determine which structure forms, dependent on the particle size, under high-pressures also.[19,20] Thus, it can be suggested that structure destabilization in response to compression along directions with greater atomic density (shorter Ti-O bonds) in anatase and TiO_2-B leads to disorder (amorphization) in the case of ultrafine crystallites and crystal-crystal phase transitions in the case of coarser crystallites. Such pressure-dependent structure destabilization is not observed in the case of rutile either experimentally or computationally to ~30 GPa.[30]

4. Conclusions

In summary, the present first-principles calculations provide an atomic-level understanding of the structural underpinnings that lead to the unusual compression behaviors and phase transitions (including amorphization) in $(Ti,Zr)O_2$ anatase and TiO_2-B. The present work has

shown that the intrinsic nature of the crystal structure in terms of Ti-O polyhedral condensation (*e.g.*, relatively higher octahedral edge-sharing in the case of anatase and TiO_2-B) ultimately determines the response of these polymorphs to pressure. The compressibility of a $(Ti,Zr)O_2$ anatase is determined by its crystallite size, composition, and the state of structural disorder. Inclusion of *P-V* data belonging to non-elastic compression regime can lead to unusual EoS parameters.

Acknowledgements

Computations were carried out at the National Computational Infrastructure – National Facility of Australia (http://nf.nci.org.au/). The author is grateful to the Advanced Engineering Platform, Monash University Malaysia for partial financial support.

Notes and references

[a]Advanced Engineering Platform, School of Engineering, Monash University Malaysia, Jalan Lagoon Selatan, Bandar Sunway, 46150 Selangor, Malaysia

[b]Department of Materials Engineering, Monash University, Clayton Campus, Victoria 3800, Australia

Corresponding Author

Email: varghese.swamy@monash.edu; Phone: +60-3-55146245; Fax: +60-3-55146207

1. P.V. Kamat (Ed.). *J. Phys. Chem. C*, 2012, **116**, 11849–11851.
2. W. Q. Fang, X.-Q. Gong and H. G. Yang, *J. Phys. Chem. Lett.*, 2011, **2**, 725-734.
3. X. Chen and S. S. Mao, *Chem. Rev.*, 2007, **107**, 2891-2959.
4. J. H. Lee and A. Selloni, *Phys. Rev. Lett.*, 2014, **112**, 196102.
5. J. Chen, Y.-F. Li, P. Sit and A. Selloni, *J. Am. Chem. Soc*., 2013, **135**, 18774−18777.
6. M. Setvin, U. Aschauer, P. Scheiber, Y.-F. Li, W. Y. Hou, M. Schmid, A. Selloni, and U. Diebold, *Science*, 2013, **341**, 988-991.
7. M. Setvin, X. Hao, B. Daniel, J. Pavelec, Z. Novotny, G. S. Parkinson, M. Schmid, G. Kresse, C. Franchini and U. Diebold, *Angew. Chem. Int. Ed*., 2014, **53**, 4714 –4716.

8. Q. Meng, Z. Guan, J. Huang, Q. Li and J. Yang, *Phys. Chem. Chem. Phys.*, 2014, **16**, 1519-11526.
9. D. B. Migas, A. B. Filonov, V. E. Borisenko and N. V. Skorodumova, *Phys. Chem. Chem. Phys.*, 2014, **16**, 9479-9489.
10. T. Brousse, R. Marchand, P. L. Taberna and P. Simon, *J. Power Sources*, 2006, **158**, 571-577.
11. M. Zukalova, M. Kalbac, L. Kavan, I. Exnar and M. Graetzel, *Chem. Mater.*, 2005, **17**, 1248-1255.
12. V. Swamy, L. S. Dubrovinsky, N. A. Dubrovinskaia, A. S. Simionovici, M. Drakapolous, V. Dmitriev and H. –P. Weber, *Solid State Commun*., 2003, **125**, 111-115.
13. V. Pischedda, G. R. Hearne, A. M. Dawe and J. E. Lowther, *Phys. Rev. Lett*., 2006, **96**, 035509.
14. S. –w. Park, J. –t. Jang, J. Cheon, H. –H. Lee, D. R. Lee and Y. Lee, *J. Phys. Chem. C*, 2008, **112**, 9627-9631.
15. V. Swamy, E. Holbig, L. S. Dubrovinsky, V. Prakapenka, B. C. Muddle, *J. Phys. Chem. Solids*, 2008, **69**, 2332-2335.
16. B. Chen, H. Zhang, K. A. Dunphy-Guzman, D. Spagnoli, M. B. Kruger, D. V. S. Muthu, M. Kunz, S. Fakra, J. Z. Zhu, Q. Z. Guo and J. F. Banfield, *Phys. Rev. B*, 2009,**79**, 125406.
17. Y. Al-Khatatbeh, K. K. M. LeeandB. Kiefer,*J. Phys. Chem. C*, 2012, **116**, 21635-21639.
18. Q. Li,B. Cheng, X. Yang, R. Liu, B. Liu, J. Liu, Z. Chen, B. Zou, T. Cui andB. Liu, *J. Phys. Chem. C*, 2013, **117**, 8516-8521.
19. V. Swamy, A. Kuznetsov, L. S. Dubrovinsky, R. A. Caruso, D. G. Shchukin and B. C. Muddle, *Phys. Rev. B*, 2005, **71**, 184302.
20. V. Swamy, A. Kuznetsov, L. S. Dubrovinsky, P. F. McMillan, V. B. Prakapenka, G. Shen andB. C. Muddle, *Phys. Rev. Lett*., 2006, **96**,135702.
21. V. Swamy, A. Y. Kuznetsov, L. S. Dubrovinsky, A. Kurnosov andV. B. Prakapenka, *Phys. Rev. Lett*., 2009, **103**, 075505.
22. E. Holbig, L. Dubrovinsky, G. Steinle-Neumann, V. Prakapenka and V. Swamy, *Z. Naturforsch. B – J. Chem. Sci*., 2006, **61**, 1577-1585.
23. E. Holbig, L. Dubrovinsky, N. Miyajima, V. Swamy, R. Wirth, V. Prakapenka and Kuznetsov, *J. Phys. Chem. Solids*, 2008, **69**, 2230-2233.
24. Q. Li, B. Liu, L. Wang, D. Li, R. Liu, B. Zou, T. Cui, G. Zou, Y. Meng, H. K. Mao *et al*. *J. Phys. Chem. Lett*., 2010, **1**, 309-314.

25. A. D. Becke,*J. Chem. Phys.*,1993, **98**, 1372-1377.
26. C. Lee, W. Yang and R. G. Parr, *Phys. Rev. B*, 1988, **37**, 785-789.
27. C. Adamo andV. Barone, *Chem. Phys. Lett.*, 1998, **298**, 113-119.
28. R. Dovesi, R. Orlando, B. Civalleri, C. Roetti, V. R. Saunders andC. M. Zicovich-Wilson, *Z. Kristallogr.*, 2005, **220**, 571-573.
29. R. Dovesi, V. R. Saunders, C. Roetti, R. Orlando, C. M. Zicovich-Wilson, F. Pascale, B. Civalleri, K. Doll, N. M. Harrison, I. J. Bush*et al*. CRYSTAL09 User's Manual, University of Torino, Torino, 2009.
30. V. Swamy andN. C. Wilson, *J. Phys. Chem. C*, 2014, **118**, 8617-8625.
31. J. Muscat, V. Swamy and N. M. Harrison, *Phys. Rev. B*, 2002, **65**, 224112.
32. M. F. Peintinger, D. V. Oliveira and T. Bredow, *J. Comp. Chem.*, 2013, **34**, 451-459.
33. http://www.crystal.unito.it/Basis_Sets/titanium.html#Ti_86411%28d31%29G_darco_unpub
34. T. Bredow, K. Jug and R. A. Evarestov, *Phys. Status Solidi B- Basic Solid State Phys.*, 2006, **243**, R10-R12.
35. http://www.crystal.unito.it/Basis_Sets/zirconium.html
36. F. Birch, *Phys. Rev.*, 1947, **71**, 809-824.
37. O. L. Anderson, *Equations of State of Solids for Geophysics and Ceramic Science* (Oxford University Press, Oxford, UK), 405 p, 1995.
38. F. Labat, P. Baranek, C. Domain, C. Minot and C. Adamo, *J. Chem. Phys.*, 2007, **126**, 154703.
39. M. B. Yahia, F. Lemoigno, T. Beuvier, J. -S. Filhol, M. Richard-Plouet, L. Brohan and M. –L. Doublet, *J. Chem. Phys.*, 2009, **130**, 204501.
40. A. Rubio-Ponce, A. Conde-Gallardo andD. Olguín, *Phys. Rev. B*, 2008, **78**, 035107.
41. H. Perron, C. Domain, J. Roques, R. Drot, E. Simoni and H. Catalette, *Theor. Chem. Acc.,* 2007, **117**, 565-574.
42. J. K. Burdett, T. Hughbanks, G. J. Miller, J. W. Richardson, Jr. and J. V. Smith, *J. Am. Chem. Soc.*, 1987, **109**, 3639-3646.
43. J. K. Dewhurst andJ. E. Lowther, *Phys. Rev. B*, 1998, **57**, 741-747.
44. M. Calatayud, P. Mori-Sánchez, A. Beltrán, A. Martín Pendás, E. Francisco, J. Andrés, and J. M. Recio, *Phys. Rev. B*, 2001,**64**, 184113.
45. T. Arlt, M. Bermejo, M. A. Blanco, L. Gerward, J.Z. Zhang, J. Staun Olsenand J. M. Recio, *Phys. Rev. B*, 2000, **61**, 14414-14419.
46. V. Swamy andL. S. Dubrovinsky, *J. Phys. Chem. Solids*, 2001, **62**, 673-675.

47. K. Momma andF. Izumi, *J. Appl. Crystallogr.*, 2011, **44**, 1272-1276.
48. X. G. Ma, P. Liang, L. Miao, S. W. Bie, C. K. Zhang, L. Xu and J. J. Jiang, *Phys. Stat. Solidi B*, 2009, **246**, 2132–2139.
49. Y. Al-Khatatbeh, K. K. M. Lee and B. Kiefer, *Phys. Rev. B*, 2009, **79**, 134114.
50. P. E. Lippens, A. V. Chadwick, A. Weibel, R. Bouchet and P. Knauth, *J. Phys. Chem. C*, 2008, **112**, 43-47.
51. M. Tournoux, R.Marchandand L. Brohan, *Progr. Solid St. Chem*., 1986, **17**, 33-52.
52. M. R. Ranade, A. Navrotsky, H. Z. Zhang, J. F. Banfield, S. H. Elder, A. Zaban, P. H. Borse, S. K. Kulkarni, G. S. Doran and H. J. Whitfield, *Proc. Natl. Acad. Sci*., 2002, **99**, 6476-6481.
53. M. W. Pitcher, S. V. Ushakov, A. Navrotsky, B. F. Woodfield, G. S. Li, J. Boerio-Goates and B. M. Tissue, *J. Amer. Ceram. Soc*., 2005, **88**, 160-167.

TOC GRAPHIC